

1 **Fourier Domain Analysis performances of a *RESPER* probe**

2
3 **Amplitude and Phase inaccuracies due to the *Round-Off* noise of *FFT* processors**

4
5 Alessandro Settimi*

6
7
8 *Istituto Nazionale di Geofisica e Vulcanologia (INGV) –*
9 *Sezione Roma 2 -*
10 *via di Vigna Murata 605, I-00143 Rome, Italy*

11
12
13
14 *Corresponding author: Dr. Alessandro Settimi

15 Tel: +39-0651860719

16 Fax: +39-0651860397

17 Email: alessandro.settimi@ingv.it

18	Index	
19		
20		
21		
22	Introduction.	5
23		
24	1. RESPER probe.	6
25		
26	2. Analogical to Digital Converter (ADC).	7
27		
28	2.1. Uniform sampling ADC.	8
29		
30	3. Fast Fourier Transform (FFT) processor and round-off noise.	10
31		
32	Appendix: round-off noise of a FFT processor.	14
33		
34	Amplitude Noise-to-Signal Ratio.	15
35		
36	Phase Noise-to-Signal Ratio.	17
37		
38	Acknowledgments.	21
39		
40	References.	22

41 **Introduction.**

42

43 Electrical resistivity and relative dielectric permittivity are two independent physical properties which
44 characterize the behaviour of bodies when these are excited by an electromagnetic field. The measurement of
45 these properties provides crucial information regarding practical uses of bodies (for example, materials that
46 conduct electricity) and for countless other purposes.

47 Some papers [Grard, 1990a,b][Grard and Tabbagh, 1991][Tabbagh et al., 1993][Vannaroni et al.
48 2004][Del Vento and Vannaroni, 2005] have proved that electrical resistivity and dielectric permittivity can
49 be obtained by measuring complex impedance, using a system with four electrodes, but without requiring
50 resistive contact between the electrodes and the investigated body. In this case, the current is made to
51 circulate in the body by electric coupling, supplying the electrodes with an alternating electrical signal of
52 *Low or Middle Frequency (LF-MF)*. In this type of investigation, the range of optimal frequencies for
53 resistivity values of the more common materials is between $\approx 10kHz$ and $\approx 1MHz$. Once complex impedance
54 has been acquired, the distributions of electrical resistivity and dielectric permittivity in the investigated body
55 are estimated using well-known algorithms of inversion techniques.

56 Applying the same principle, but limited to the acquisition only of resistivity, there are various
57 commercial instruments used in geology for investigating the first 2-5 meters underground both for the
58 exploration of environmental areas and archaeological investigation [Samouëlian et al., 2005].

59 As regards the direct determination of the permittivity in subsoil, omitting geo-radar which provides
60 an estimate by complex measurement procedures on radar-gram processing [Declerk, 1995][Sbartai et al.,
61 2006], the only technical instrument currently used is the so-called *Time-Domain Reflectometer (TDR)*,
62 which utilizes two electrodes inserted deep in the ground in order to acquire this parameter for further
63 analysis [Mojid et al., 2003][Mojid and Cho, 2004].

64 **1. RESPER probe.**

65

66 Previous papers [Settimi et al., 2009-2010, a-c] presented a discussion of theoretical modelling and
67 moved towards a practical implementation of a *RESPER* probe which acquires complex impedance in the
68 field. A *RESPER* allows measurement of electrical RESistivity and dielectric PERmittivity using alternating
69 current at LFs ($30kHz < f < 300kHz$) or MFs ($300kHz < f < 3MHz$). By increasing the distance between the
70 electrodes, it is possible to investigate the electrical properties of sub-surface structures to greater depth. In
71 appropriate arrangements, measurements can be carried out with the electrodes slightly raised above the
72 surface, enabling completely non-destructive analysis, although with greater error. The probe can perform
73 immediate measurements on materials with high resistivity and permittivity, without subsequent stages of
74 data analysis.

75 The paper [Settimi et al, 2009, b] has moved towards the practical implementation of electrical
76 spectroscopy. In order to design a *RESPER* probe which measures the electrical resistivity and dielectric
77 permittivity with inaccuracies below a prefixed limit (10%) in a band of LFs ($B=100kHz$), the *RESPER*
78 should be connected to an appropriate *Analogical to Digital Converter (ADC)*, which samples in uniform or
79 in *Phase and Quadrature (IQ)* mode [Jankovic and Öhman, 2001]. If the probe is characterized by a galvanic
80 contact with the surface, then the inaccuracies in the measurement of resistivity and permittivity, due to the
81 uniform or IQ sampling ADC, can be analytically expressed. A large number of numerical simulations have
82 proved that the performance depends on the selected sampler and that the IQ is preferable when compared to
83 the uniform mode under the same operating conditions, i.e. number of bits and medium.

84 This report proposes to discuss the Fourier domain analysis performances of a *RESPER* probe. A
85 uniform ADC, which is characterized by a sensible phase inaccuracy depending on frequency, is connected
86 to a *Fast Fourier Transform (FFT)* processor, that is especially affected by a *round-off* amplitude noise
87 linked to both the FFT register length and samples number. If the register length is equal to 32 bits, then the
88 round-off noise is entirely negligible, else, once bits are reduced to 16, a technique of compensation must
89 occur. In fact, oversampling can be employed within a short time window, reaching a compromise between
90 the needs of limiting the phase inaccuracy due to ADC and not raising too much the number of averaged FFT
91 values sufficient to bound the round-off.

92 Finally, the appendix presents an outline of somewhat lengthy demonstrations needed to calculate the
93 amplitude and especially phase inaccuracies due to the round-off noise of FFT processors.

94 **2. Analogical to Digital Converter (ADC).**

95
96 Typically, an ADC is an electronic device that converts an input analogical voltage (or current) to a
97 digital number [Razavi, 1995]. A sampler has several sources of errors. Quantization error and (assuming the
98 sampling is intended to be linear) non-linearity is intrinsic to any analogical-to-digital conversion. There is
99 also a so-called *aperture error* which is due to *clock jitter* and is revealed when digitizing a time-variant
100 signal (not a constant value). The accuracy is mainly limited by quantization error. However, a faithful
101 reproduction is only possible if the sampling rate is higher than twice the highest frequency of the signal.
102 This is essentially what is embodied in the Shannon-Nyquist sampling theorem.

103 There are currently a huge number of papers published in scientific literature, and the multifaceted
104 nature of each one makes it difficult to present a complete overview of the ADC models available today.
105 Technological progress, which is rapidly accelerating, makes this task even harder. Clearly, models of
106 advanced digitizers must match the latest technological characteristics. Different users of sampler models are
107 interested in different modelling details, and so numerous models are proposed in scientific literature: some
108 of them describe specific error sources [Polge et al., 1975]; others are devised to connect conversion
109 techniques and corresponding errors [Arpaia et al., 1999][Arpaia et al., 2003]; others again are devoted to
110 measuring the effect of each error source in order to compensate it [Björzell and Händel, 2008]. Finally,
111 many papers [Kuffel et al., 1991][Zhang and Ovaska, 1998] suggest general guidelines for different models.
112

113 In order to design a RESPER probe (Fig. 1.a) which measures the electrical conductivity σ and the
114 dielectric permittivity ϵ_r of a subjacent medium with inaccuracies below a prefixed limit (10%) in a band of
115 LFs ($B=100kHz$), the RESPER can be connected to an appropriate ADC, with bit resolution not exceeding
116 12, thereby rendering the probe (voltage scale of 4V) almost insensitive to the electric noise of the external
117 environment ($\approx 1mV$) [Settimi et al., 2009-2010, a-c].

118 With the aim of investigating the physics of the measuring system, the inaccuracies in the complex
119 impedance measured by the RESPER (Fig. 1.b) are provided.

120 In the stage downstream of the probe, the electrical voltage V is amplified $V_V=A_V \cdot V$, then the intensity of
121 current I is transformed by a trans-resistance amplifier $V_I=A_R \cdot I$, and finally these signals are processed by the
122 sampler. It follows that:

123 the inaccuracy $\Delta|Z|/|Z|$ for the amplitude of the complex impedance results from the negligible
124 contributes $\Delta A_V/A_V$ and $\Delta A_R/A_R$, respectively for the voltage and trans-resistance amplifiers, and the
125 predominant one $\Delta|V_V|/|V_V|$ for the amplitude of the voltage, due to the sampling,

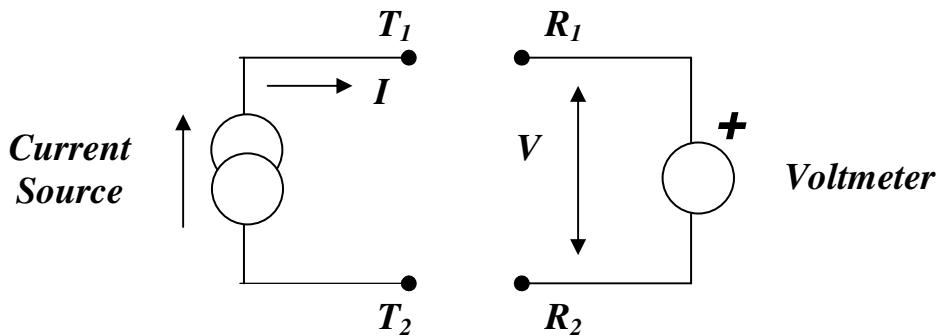
$$\frac{\Delta|Z|}{|Z|} = \frac{\Delta A_V}{A_V} + \frac{\Delta A_R}{A_R} + 2 \frac{\Delta|V_V|}{|V_V|} \cong 2 \frac{\Delta|V_V|}{|V_V|}, \quad (2.1)$$

127 the inaccuracies for the amplitude of the voltage and the current intensity being equal, $\Delta|V_V|/|V_V| = \Delta|V_I|/|V_I|$;

128 instead, the inaccuracy $\Delta\Phi_Z/\Phi_Z$ for the initial phase of the complex impedance coincides with the one
129 $\Delta\varphi_V/\varphi_V$ for the phase of the voltage, due to the sampler,

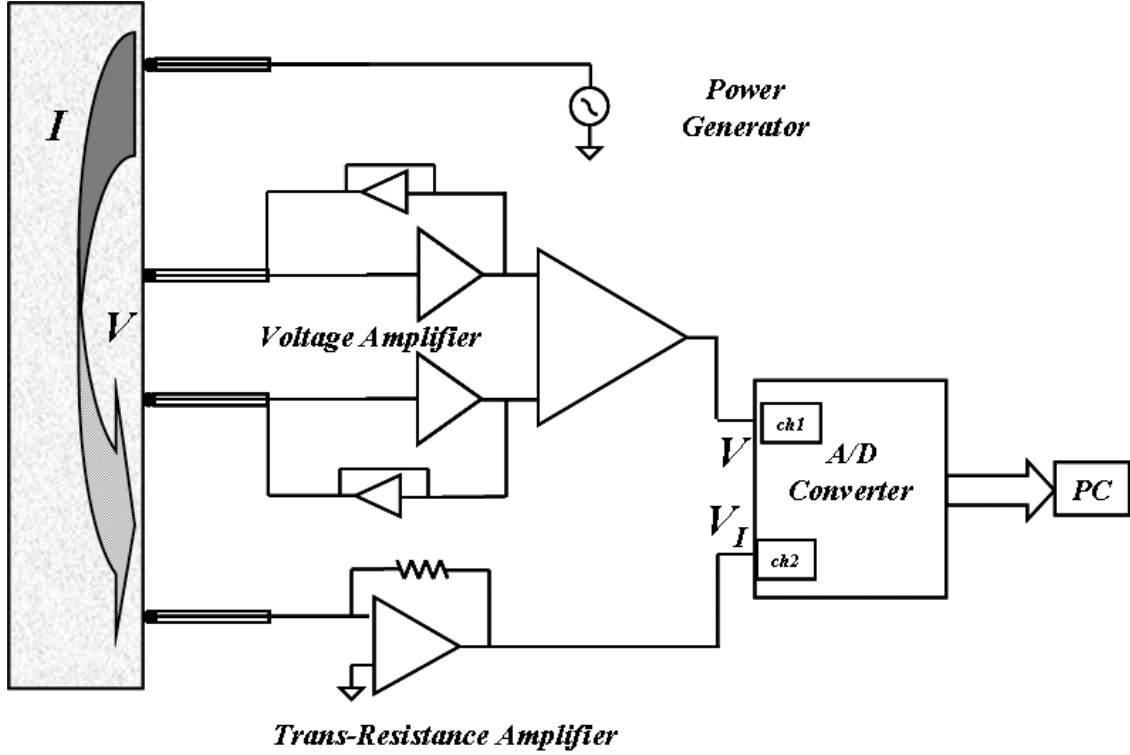
$$\frac{\Delta\Phi_Z}{\Phi_Z} = \frac{\Delta\varphi_V}{\varphi_V}, \quad (2.2)$$

131 the initial phase of the current being null, $\varphi_I=0$.



133
134
135 **Figure 1.a.** Equivalent circuit of a RESPER probe.

136
137
138
139
140
141
142
143
144
145
146
147
148
149



150
151
152
153
154
155
156
157
158
159
160
161
162

Figure 1.b. Block diagram of the measuring system, which is composed of: a series of four electrodes laid on the material to be investigated; an analogical circuit for the detection of signals connected to a high voltage sinusoidal generator; a digital acquisition system; and a personal computer. Starting from the left, the four electrodes can be seen laid on the block of material to be analyzed. Two electrodes are used to generate and measure the injected current (at a selected frequency), while the other two electrodes are used to measure the potential difference. In this way, two voltages are obtained: the first proportional to the current; the second proportional to the difference of potential. These voltages are digitized through an *Analogical to Digital converter* (ADC) connected to a personal computer for further processing. The real magnitudes hereby measured in the time domain are subsequently transformed into complex magnitudes in the frequency domain. From the ratio of the complex values, at the specific investigated frequency, it is possible to obtain the complex impedance. A program with an algorithm of numerical inversion allows the electrical resistivity and dielectric permittivity of the material to be obtained by measuring the complex impedance; in this way, the reliability of the measured data is immediately analyzed, proving very useful during a measurement program.

163
164

2.1. Uniform sampling ADC.

165
166
167

As concerns uniform sampling [Razavi, 1995], the inaccuracy $\Delta|Z|/|Z|_U(n)$ for $|Z|$ depends only on the bit resolution n , decreasing as the exponential function 2^{-n} of n (Fig. 2.a),

168

$$\frac{\Delta|Z|}{|Z|_U} = \frac{1}{2^n}. \quad (2.3)$$

169
170
171

Instead, the inaccuracy $\Delta\Phi_Z/\Phi_Z|_U(f,f_s)$ for Φ_Z depends on both the working frequency f of the RESPER and the rate sampling f_s of the ADC, the inaccuracy being directly proportional to the frequency ratio f/f_s (Fig. 2.b),

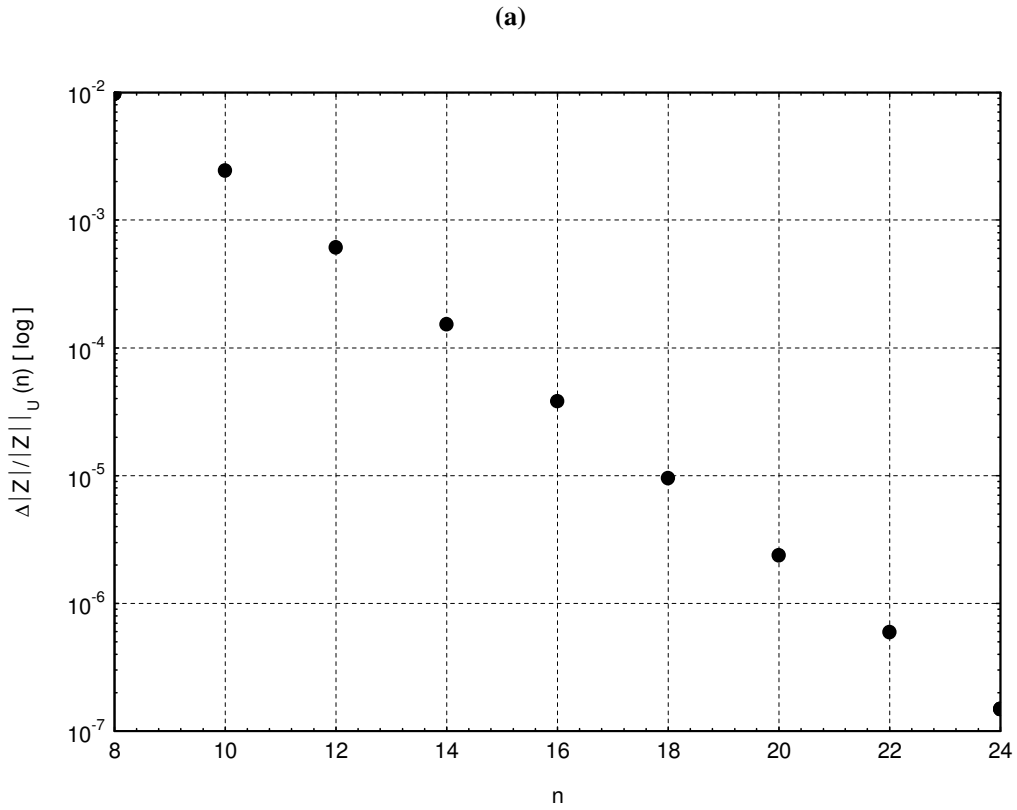
172

$$\frac{\Delta\Phi_Z}{\Phi_Z|_U} = 2 \frac{f}{f_s}. \quad (2.4)$$

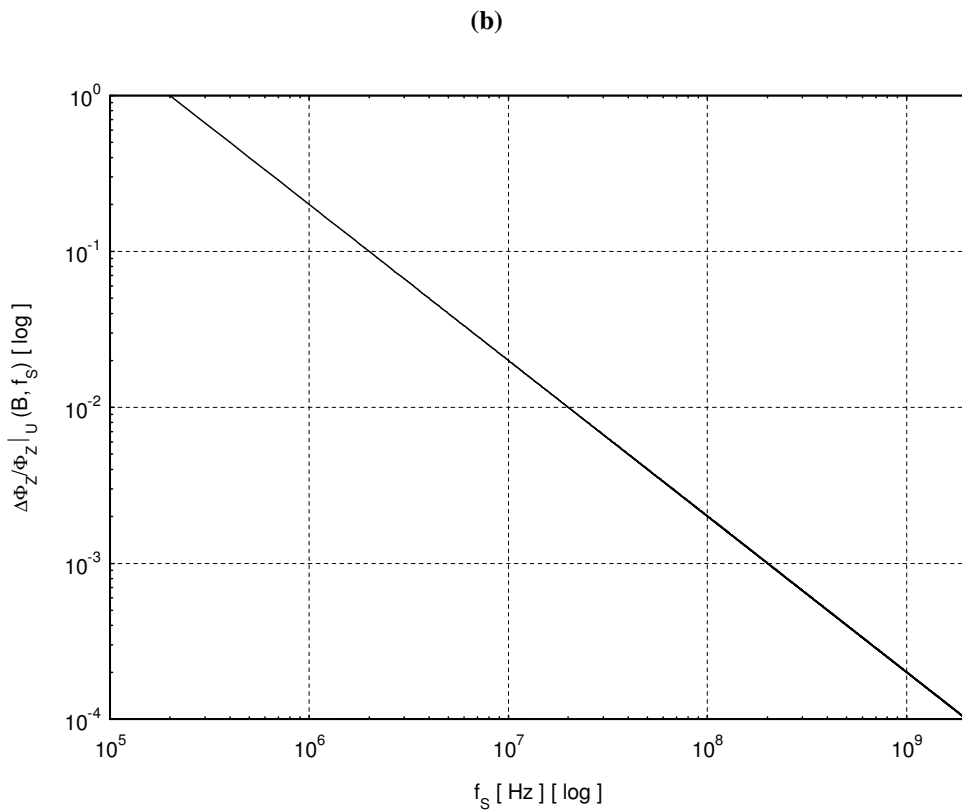
173
174
175

As a consequence, for uniform sampling ADCs, the inaccuracy $\Delta\Phi_Z/\Phi_Z|_U(f,f_s)$ for the phase Φ_Z must be optimized in the upper frequency f_{up} , so when the probe performs measurements at the limit of its band B , i.e. $f_{up}=B$.

176
177



178
179
180
181



182
183
184
185
186
187
188

Figure 2. A class of uniform ADCs is specified by bit resolution n , ranging from 8 bit to 24 bit, and rate sampling f_s , in the band of frequency [500 kHz, 2GHz]: (a) semi-logarithmic plot for the inaccuracy $\Delta|Z|/|Z|_U(n)$ in the measurement of the amplitude for complex impedance, as a function of the resolution n ; (b) Bode's diagram for the inaccuracy $\Delta\Phi_Z/\Phi_Z|_U(B, f_s)$ of the complex impedance in phase, plotted as a function of the rate f_s , when the RESPER works in the upper frequency at the limit of its band $B=100kHz$.

189 **3. Fast Fourier Transform (FFT) processor and round-off noise.**
 190

191 In mathematics, the *Discrete Fourier Transform (DFT)* is a specific kind of Fourier transform, used in
 192 Fourier analysis. The DFT requires an input function that is discrete and whose non-zero values have a
 193 limited (finite) duration. Such inputs are often created by sampling a continuous function. Using the DFT
 194 implies that the finite segment which is analyzed is one period of an infinitely extended periodic signal; if
 195 this is not actually true, a window function has to be used to reduce the artefacts in the spectrum. In
 196 particular, the DFT is widely employed in signal processing and related fields to analyze the frequencies
 197 contained in a sampled signal. A key enabling factor for these applications is the fact that the DFT can be
 198 computed efficiently in practice using a *Fast Fourier Transform (FFT)* algorithm [Oppenheim et al., 1999].

199 It is important to understand the effects of finite register length in the computation. Specifically,
 200 arithmetic *round-off* is analyzed by means of a linear-noise model obtained by inserting an additive noise
 201 source at each point in the computation algorithm where round-off occurs. However, the effects of round-off
 202 noise are very similar among the different classes of FFT algorithms.
 203

204 Generally, a FFT processor which computes N samples, represented as $n_{FFT}+1$ bit signed fractions, is
 205 affected by a round-off noise which is added to the inaccuracy for complex impedance, in amplitude
 206 [Oppenheim et al., 1999][see Appendix]

207
$$\left. \frac{\Delta|Z|}{|Z|} \right|_{Round-off} = \frac{N}{2^{n_{FFT}-1}}, \quad (3.1)$$

208 and in phase [Dishan, 1995][Ming and Kang, 1996][see Appendix],

209
$$\left. \frac{\Delta\Phi_Z}{\Phi_Z} \right|_{Round-off} = \frac{1}{\pi\sqrt{N}2^{n_{FFT}}}. \quad (3.2)$$

210 So, maximizing the register length to $n_{FFT}=32$, the round-off noise is entirely negligible. Once that
 211 $n_{FFT}<32$, if the number of samples is increased $N \gg 1$, then the round-off noise due to FFT degrades the
 212 accuracy of complex impedance, so much more in amplitude (3.1) how much less in phase (3.2).

213 One can overcome this inconvenience by iterating the FFT processor for A cycles, as the best estimate
 214 of one FFT value is the average of A FFT repeated values. The improvement is that the inaccuracy for the
 215 averaged complex impedance, in amplitude and phase, consists of the error of quantization due to the
 216 uniform sampling ADC (2.3)-(2.4) and on the round-off noise due to FFT (3.1)-(3.2), the last term being
 217 decreased of \sqrt{A} , i.e.:

218
$$\frac{\Delta|Z|}{|Z|} = \frac{\Delta|Z|}{|Z|} \Big|_U + \frac{1}{\sqrt{A}} \left. \frac{\Delta|Z|}{|Z|} \right|_{Round-off} = \frac{1}{2^n} + \frac{1}{\sqrt{A}} \frac{N}{2^{n_{FFT}-1}}, \quad (3.3)$$

219
$$\frac{\Delta\Phi_Z}{\Phi_Z} = \frac{\Delta\Phi_Z}{\Phi_Z} \Big|_U + \frac{1}{\sqrt{A}} \left. \frac{\Delta\Phi_Z}{\Phi_Z} \right|_{Round-off} = 2 \frac{f}{f_s} + \frac{1}{\sqrt{A}} \frac{1}{\pi\sqrt{N}2^{n_{FFT}}}. \quad (3.4)$$

220 Once reduced the register length to $n_{FFT} \leq 16$, only if the FFT processor performs the averages during a
 221 number of cycles

222
$$\left(\frac{N}{2^{n_{FFT}-n-1}} \right)^2 \ll A \leq N^2, \quad (3.5)$$

223 then the round-off noise due to FFT can be neglected with respect to the quantization error due to uniform
 224 ADC, in amplitude

225
$$\frac{\Delta|Z|}{|Z|} \cong \frac{1}{2^n} + \frac{1}{2^{n_{FFT}-1}} \approx \left. \frac{\Delta|Z|}{|Z|} \right|_U = \frac{1}{2^n}, \quad (3.6)$$

226 and especially in phase

227
$$\frac{\Delta\Phi_Z}{\Phi_Z} \cong 2 \frac{f}{f_s} + \frac{1}{\pi N \sqrt{N} 2^{n_{FFT}}} \approx \left. \frac{\Delta\Phi_Z}{\Phi_Z} \right|_U = 2 \frac{f}{f_s}. \quad (3.7)$$

228 So, the round-off noise due to FFT is compensated. The quantization error due to ADC decides the
 229 accuracy for complex impedance: it is constant in amplitude, once fixed the bit resolution n , and can be
 230 limited in phase, by an oversampling technique $f_s \gg f$.

231 In the limit of the Shannon-Nyquist theorem, an electric signal with band of frequency B must be
 232 sampled at the minimal rate $f_s = 2B$, holding N_{min} samples in a window of time T . Instead, in the hypothesis
 233 of oversampling, the signal can be sampled holding the same number of samples N_{min} but in a shorter time
 234 window T/R_o , due to an high ratio of sampling:

$$235 \quad R_o = \frac{f_s}{2B} \gg 1. \quad (3.8)$$

236 This is equivalent to the operating condition such that, during the time window,

$$237 \quad T = \frac{N_{min}}{2B}, \quad (3.9)$$

238 the uniform over-sampling ADC holds a samples number

$$239 \quad N = R_o \cdot N_{min} \gg N_{min} \quad (3.10)$$

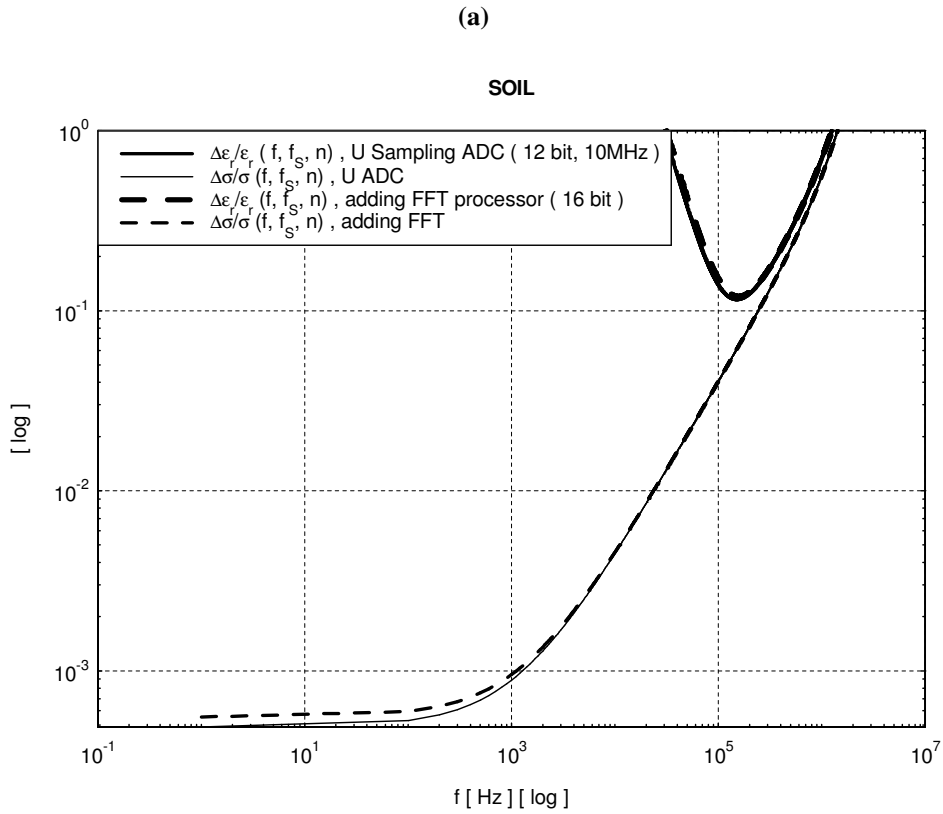
240 which is linked to the number of cycles iterated by the FFT processor:

$$241 \quad A \cong N^2 = R_o^2 \cdot N_{min}^2 \gg 1. \quad (3.11)$$

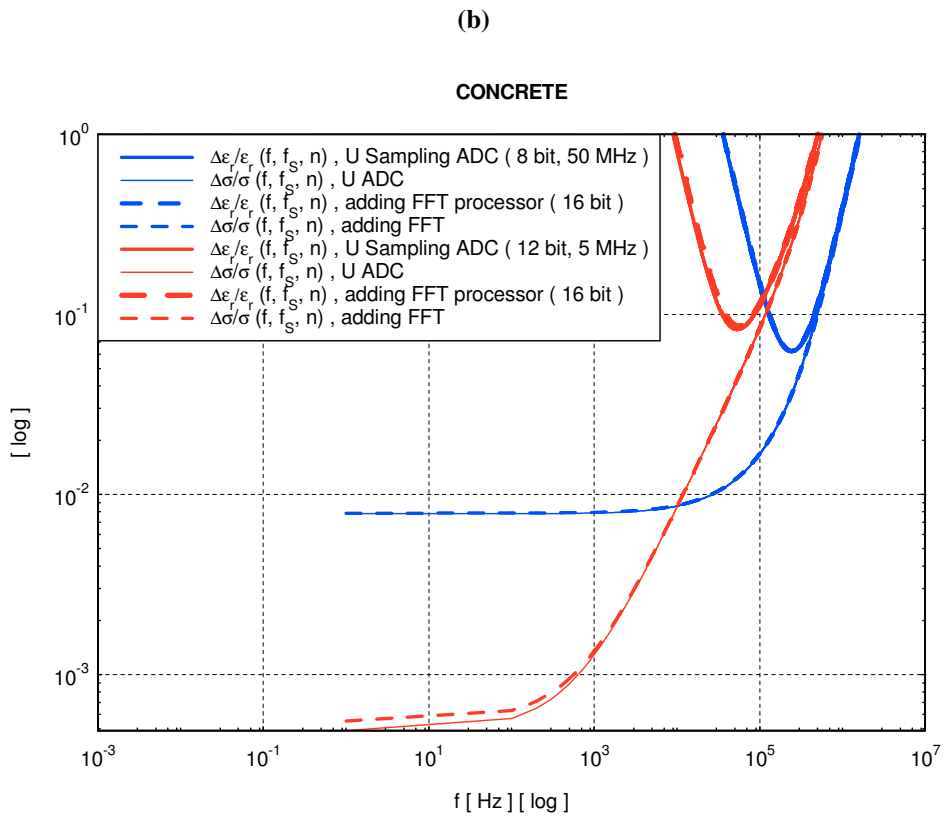
242 As comments on eqs. (3.9)-(3.11), a low number of samples N_{min} , corresponding to the Shannon-
 243 Nyquist limit, shortens the time window (3.9). An high oversampling ratio lowers the phase inaccuracy
 244 although it raises the samples number hold by uniform ADC and especially the cycles number iterated by
 245 FFT; however, even a minimal oversampling ratio $R_{o,min}$ limits the phase inaccuracy with the advantage of
 246 not raising too much the samples number hold by ADC (3.10) and especially the cycles number iterated by
 247 FFT (3.11).

248
 249 A RESPER probe (frequency band B) shows a galvanic contact with the subjacent non-saturated
 250 medium (terrestrial soil or concrete with low dielectric permittivity, $\epsilon_r = 4$, and high electrical resistivity,
 251 $1/\sigma_s = 3 \cdot 10^3 \Omega \cdot m$, $1/\sigma_c = 1 \cdot 10^4 \Omega \cdot m$). It is required that the inaccuracy $\Delta\epsilon_r/\epsilon_r(f, f_s, n)$ in the measurement of
 252 permittivity ϵ_r is below a prefixed limit $\Delta\epsilon_r/\epsilon_r|_{fixed}$ (10% ÷ 15%) within the band B (100kHz). As a first result,
 253 if the samples number satisfying the Shannon-Nyquist theorem is minimized, i.e. $N_{min}=2$, then the time
 254 window for sampling is shortened to $T = N_{min}/(2B) = 1/B \approx 10\mu s$. In order to analyze the complex impedance
 255 measured by the RESPER in Fourier domain, a uniform ADC can be connected to a FFT processor, being
 256 affected by a round-off amplitude noise. As a conclusive result, a technique of compensation must occur.
 257 The ADC must be specified by: a minimal bit resolution $n \leq 12$, thereby rendering the probe almost
 258 insensitive to the electric noise of the external environment; and a minimal over-sampling rate f_s , which
 259 limits the ratio $R_o = f_s/(2B)$, so the actual samples number $N = R_o \cdot N_{min}$ is up to one hundred (soil, $f_s = 10MHz$,
 260 $R_o = 50$, $N \approx 100$)(concrete, $f_s = 5MHz$, $R_o = 25$, $N \approx 50$). Moreover, even if the FFT register length is equal
 261 to $n_{FFT} = 16$, anyway the minimal rate f_s ensures a number of averaged FFT values $A \leq N^2$ even up to ten
 262 thousand, necessary to bound the round-off noise (soil, $A \approx 10^4$)(concrete, $A \approx 2.5 \cdot 10^3$) (Fig. 3)(Tab. 1)
 263 [Settimi et al., 2009-2010, a-c].

264
265



266
267
268
269



270
271
272
273
274
275
276

Figure 3. The probe is connected to an uniform ADC of minimal bit resolution $n \leq 12$ and over-sampling rate f_s , (12 bit, 10 MHz)(a) and (8 bit, 50 MHz) or (12 bit, 5 MHz)(b), in addition to a Fast Fourier Transform (FFT) processor of register length $n_{FFT} = 16$ which ensures inaccuracies $\Delta \epsilon_r / \epsilon_r(f)$ and $\Delta \sigma / \sigma(f)$ in the measurement of permittivity ϵ_r , and conductivity σ below a prefixed limit, 15% referring to (a) and 10% for (b), within the frequency band $B = 100 \text{ kHz}$ (Tab. 1) [Settimi et al., 2009-2010, a-c].

277
278

(a)

Soil ($\epsilon_r = 4$, $\rho = 3000 \Omega \cdot m$)	U Sampling ADC ($n = 12$, $f_s = 10 \text{ MHz}$) + FFT ($n_{\text{FFT}} = 16$)
$T = N_{\text{min}}/2B$	$\approx 10 \mu\text{s}$
$N = N_{\text{min}} \cdot (f_s/2B)$	$\approx 100 (2^7 = 128)$
$A \leq N^2$	$\approx 10^4$
$f_{\text{opt}}, f_{\text{min}}, f_{\text{max}}$ ($\Delta\epsilon_r/\epsilon_r, \Delta\sigma/\sigma \leq 0.15$)	156.256 kHz, 99.68 kHz, 261.559 kHz

279
280
281

(b)

Concrete ($\epsilon_r = 4$, $\rho = 10000 \Omega \cdot m$)	U Sampling ADC ($n = 8$, $f_s = 50 \text{ MHz}$) + FFT ($n_{\text{FFT}} = 16$)	U Sampling ADC ($n = 12$, $f_s = 5 \text{ MHz}$) + FFT ($n_{\text{FFT}} = 16$)
$T = N_{\text{min}}/2B$	$\approx 10 \mu\text{s}$	
$N = N_{\text{min}} \cdot (f_s/2B)$	$\approx 500 (2^9 = 512)$	$\approx 50 (2^6 = 64)$
$A \leq N^2$	$\approx 2.5 \cdot 10^5$	$\approx 2.5 \cdot 10^3$
$f_{\text{opt}}, f_{\text{min}}, f_{\text{max}}$ ($\Delta\epsilon_r/\epsilon_r, \Delta\sigma/\sigma \leq 0.15$)	241.906 kHz, 99.007kHz, 591.411 kHz ($\Delta\epsilon_r/\epsilon_r, \Delta\sigma/\sigma \leq 0.15$)	55.344 kHz, 38.195kHz, 83.642 kHz ($\Delta\epsilon_r/\epsilon_r, \Delta\sigma/\sigma \leq 0.1$)

282
283
284
285
286

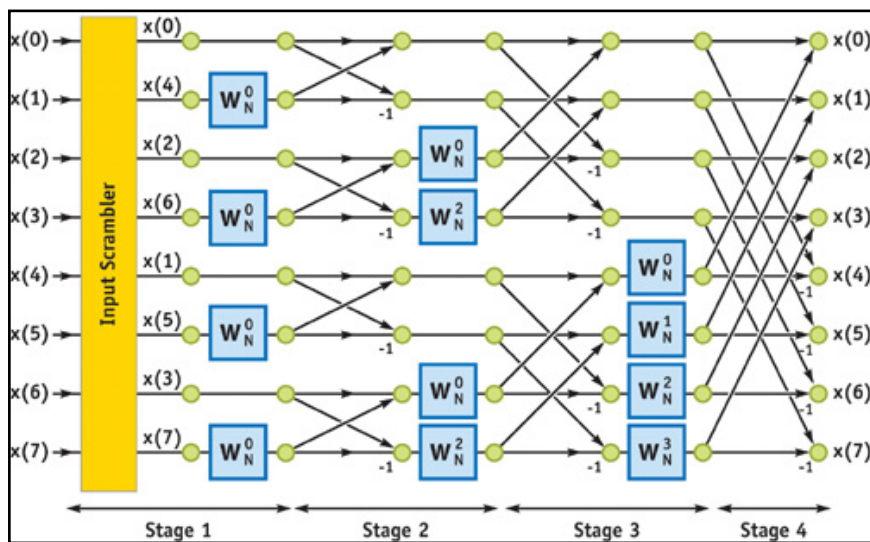
Table 1. Refer to the caption of fig. 3. A RESPER probe is connected to an uniform ADC (Shannon-Nyquist theorem: limit of samples number, $N_{\text{min}} = 2$), in addition to a FFT processor with *round-off* noise (T , time window; N , actual samples number; A , cycles number averaging FFT values). Optimal, minimum and maximum working frequencies, f_{opt} , f_{min} and f_{max} , for measurements performed on terrestrial soil (a) and concrete (b) [Settimi et al., 2009-2010, a-c].

287 **Appendix: round-off noise of a FFT processor.**
 288

289 The *Discrete Fourier Transform (DFT)* plays an important role in the analysis, design, and
 290 implementation of discrete-time signal-processing algorithms and systems [Oppenheim et al., 1999]. The
 291 basic properties of the Fourier transform and discrete Fourier transform make it particularly convenient to
 292 analyze and design systems in the Fourier domain. Equally important is the fact that efficient algorithms
 293 exist for explicitly computing the DTF. As a result, the DTF is an important component in many practical
 294 applications of discrete-time systems.

295 As discussed in Oppenheim (1999), the DTF is identical to samples of the Fourier transform at equally
 296 spaced frequencies. Consequently, computation of the N -point DTF corresponds to the computation of the N
 297 samples of the Fourier transform at N equally spaced frequencies, $\omega_k=2\pi k/N$, i.e. at N points on the unit
 298 circle in the complex plane. Oppenheim considers techniques for computation of the discrete Fourier
 299 transform. The periodicity and symmetry of the complex factor $W_N^{kn} = e^{-j(2\pi/N)kn}$ can be exploited to
 300 increase the efficiency of DFT computations. However, the major emphasis is on *Fast Fourier Transform*
 301 (*FFT*) algorithms. The *decimation-in-time* and *decimation-in-frequency* classes of FFT algorithms are
 302 described in some detail, and even some of the implementation considerations, such as indexing and
 303 coefficient quantization. Much of the detailed discussion concerns algorithms that require N to be a power of
 304 2, since these algorithms are easy to understand, simple to program, and most often used.

305 Oppenheim (1999) has discussed effects of finite word length in DFT computations. Linear-noise
 306 models are used to show that the *Noise-to-Signal Ratio* of a DFT computation varies differently with the
 307 length of the sequence, depending on how scaling is done. Oppenheim also comments briefly on the use of
 308 floating-point representations.
 309



310
 311
 312 Figure 4. Flow graph for decimation-in-time FFT algorithm.
 313

314 **Amplitude Noise-to-Signal Ratio.**

315

316 A flow graph depicting the decimation-in-time algorithm for $N=8$ is shown in fig. 4. Some key aspects
 317 of this diagram are common to all standard radix-2 algorithms. The DFT is computed in $v=\log_2 N$ stages. At
 318 each stage a new array of N numbers is formed from the previous array by linear combinations of the
 319 elements, taken two at a time. The v -th array contains the desired DFT.

320 The round-off noise is modelled by associating an additive noise generator with each fixed-point
 321 multiplication [Oppenheim et al., 1999].

322

323 Since, in general, the input to the FFT is a complex sequence, each of the multiplications is complex
 324 and thus consists of four real multiplications. Assume that the errors due to each real multiplication have the
 325 following properties:

- 326 1. The errors are uniformly distributed random variables over the range $-(1/2) \cdot 2^{n_{FFT}}$ to $+(1/2) \cdot 2^{n_{FFT}}$,
 327 where numbers are represented as $(n_{FFT}+1)$ -bit signed fractions. Therefore, each error source has
 328 variance $2^{-2n_{FFT}}/12$.
 329 2. The errors are uncorrelated with one another.
 330 3. all the errors are uncorrelated with the input and, consequently, also with the output.

331 Since each of the four noise sequences is uncorrelated zero-mean white noise and all have the same
 332 variance,

333
$$\sigma_{n_{FFT}}^2 = 4 \cdot \frac{2^{-2n_{FFT}}}{12} = \frac{1}{3} \cdot 2^{-2n_{FFT}}. \quad (\text{A.1})$$

334 To determine the mean-square value of the output noise at any output node, one must account for the
 335 contribution from each of the noise sources which propagate to that node.

336 The following observations can be made from the flow graph of fig. 4:

- 337 1. The transmission function from any node in the flow graph to any other node to which it is
 338 connected is multiplied by a complex constant of unit magnitude (because each branch
 339 transmittance is either unity or an integer power of W_N).
 340 2. Each output node connects to seven butterflies in the flow graph. In general, each output node would
 341 connect to $(N-1)$ butterflies.

342 These observations can be generalized to the case of N an arbitrary power of 2.

343 With these assumptions, then, the mean square value of the output noise in the k -th DFT value, $F[k]$, is
 344 given by [Oppenheim et al., 1999]

345
$$\langle |F[k]|^2 \rangle = (N-1) \sigma_{n_{FFT}}^2, \quad (\text{A.2})$$

346 which, for large N , can be approximated as:

347
$$\langle |F[k]|^2 \rangle \cong N \sigma_{n_{FFT}}^2. \quad (\text{A.3})$$

348 According to this result, the mean square value of the output noise is proportional to N , the number of
 349 points transformed. The effect of doubling N , or adding another stage in the FFT, is to double the mean-
 350 square value of the output noise. Note that for FFT algorithms, a double-length accumulator does not help to
 351 reduce round-off noise, since the outputs of the butterfly computation must be stored in $(n_{FFT}+1)$ -bit registers
 352 at the output of each stage.

353

354 In implementing an FFT algorithm with fixed-point arithmetic, one must ensure against overflow. If
 355 the magnitude of the output of the FFT is less than unity, then the magnitude of the points in each array must
 356 be less than unity, i.e. there will be no overflow in any of the arrays.

357 To express this constraint as a bound on the input sequence, note that the condition

358
$$|x[n]| < \frac{1}{N}, \quad 0 \leq n \leq N-1, \quad (\text{A.4})$$

359 is both necessary and sufficient to guarantee that

360
$$|X[k]| < 1, \quad 0 \leq k \leq N-1. \quad (\text{A.5})$$

361 This follows from the definition of the DFT, since:

362
$$|X[k]| = \left| \sum_{n=0}^{N-1} x[n] W_N^{kn} \right| \leq \left| \sum_{n=0}^{N-1} x[n] \right|, \quad k = 0, 1, \dots, N-1. \quad (\text{A.6})$$

363 Then eq. (A.4) is sufficient to guarantee that there will be no overflow for all stages of algorithm.

364 To obtain an explicit expression for the Noise-to-Signal Ratio at the output of the FFT algorithm,
 365 consider an input in which successive sequence values are uncorrelated, i.e. a white-noise input signal. Also,
 366 assume that the real and imaginary parts of the input sequence are uncorrelated and that each has an amplitude
 367 density which is uniform between $-1/(\sqrt{2} N)$ and $+1/(\sqrt{2} N)$ [Note that this signal satisfies eq. (A.4)].
 368 Then the average squared magnitude of the complex input sequence is:

369
$$\sigma_x^2 = \langle |x[n]|^2 \rangle = \frac{1}{3N^2}. \quad (\text{A.7})$$

370 The DTF of the input sequence is

371
$$X[k] = \sum_{n=0}^{N-1} x[n] W_N^{kn}, \quad (\text{A.8})$$

372 from which it can be shown that, under the foregoing assumptions on the input,

373
$$\langle |X[k]|^2 \rangle = \sum_{n=0}^{N-1} \langle |x[n]|^2 \rangle |W_N^{kn}|^2 = N\sigma_x^2 = \frac{1}{3N}. \quad (\text{A.9})$$

374 Combining eqs. (A.3) and (A.9), it is obtained [see eq. (3.1)]:
 375

376
$$\frac{\langle |F[k]|^2 \rangle}{\langle |X[k]|^2 \rangle} \cong 3N^2 \sigma_{n_{FFT}}^2 = N^2 2^{-2n_{FFT}}. \quad (\text{A.10})$$

377 According to eq. (A.10), the noise-to-signal ratio increases as N^2 , or 1 bit per stage. That is, if N is
 378 doubled, corresponding to adding one additional stage to the FFT, then to maintain the same noise-to-signal
 379 ratio, 1 bit must be added to the register length. The assumption of a white-noise input signal is, in fact, not
 380 critical here. For a variety of other inputs, the noise-to-signal ratio is still proportional to N^2 , with only the
 381 constant of proportionality changing.
 382

383 The preceding analysis shows that scaling to avoid overflow is the dominant factor in determining the
 384 noise-to-signal ratio of fixed-point implementations of FFT algorithms. Therefore, floating-point arithmetic
 385 should improve the performances of these algorithms. The effect of floating point round-off on the FFT is
 386 analyzed both theoretically and experimentally by Gentleman and Sande (1966), Weinstein (1969), and
 387 Kaneko and Liu (1970) (see references therein [Oppenheim et al., 1999]). The investigations show that, since
 388 scaling is no longer necessary, the decrease of noise-to-signal ratio with increasing N is much less dramatic
 389 than for fixed-point arithmetic.

390 For example, Weinstein (1969) showed theoretically that the noise-to-signal ratio is proportional to v
 391 for $N=2^v$, rather than proportional to N as in the fixed-point case. Therefore, quadrupling v (raising N to the
 392 fourth power) increases the noise-to-signal ratio by only 1 bit.

393 **Phase Noise-to-Signal Ratio.**

394

395

Firstly, let us consider the k -th value of the DTF

$$396 \quad X[k] = \sum_{n=0}^{N-1} x[n] W_N^{kn} = \sum_{n=0}^{N-1} x[n] e^{-j(2\pi/N)kn}, \quad k = 0, 1, \dots, N-1, \quad (\text{A.11})$$

397

corresponding to a complex sequence:

$$398 \quad x[n] = x_R[n] + jx_I[n] = |x[n]| e^{j\varphi[n]}, \quad n = 0, 1, \dots, N-1. \quad (\text{A.12})$$

399

The phase $\Phi[k]$ of the k -th DFT value $X[k] = |X[k]| e^{j\Phi[k]}$ can be calculated as

$$400 \quad \Phi[k] = \text{Im} \ln X[k], \quad (\text{A.13})$$

401

instead the phase $\varphi[n] - (2\pi/N)kn$ of the n -th sequence term $x[n] e^{-j(2\pi/N)kn} = |x[n]| e^{j\varphi[n]} e^{-j(2\pi/N)kn}$ as:

$$402 \quad \varphi[n] - \frac{2\pi}{N} kn = \text{Im} \ln \{ x[n] e^{-j(2\pi/N)kn} \}. \quad (\text{A.14})$$

403

Applying a special inequality

$$404 \quad \text{Im} \sum_{n=0}^{N-1} x[n] e^{-j(2\pi/N)kn} \leq \frac{1}{N} \sum_{n=0}^{N-1} \text{Im} \{ x[n] e^{-j(2\pi/N)kn} \}, \quad (\text{A.15})$$

405

the phase $\Phi[k]$ of the k -th DFT value (A.11) can be superiorly limited by the sum of phases $\varphi[n]$ for the complex sequence (A.12):

406

$$\Phi[k] = \text{Im} \ln X[k] = \text{Im} \ln \sum_{n=0}^{N-1} x[n] e^{-j(2\pi/N)kn} \leq$$

407

$$\leq \frac{1}{N} \sum_{n=0}^{N-1} \text{Im} \ln \{ x[n] e^{-j(2\pi/N)kn} \} = \frac{1}{N} \sum_{n=0}^{N-1} \left\{ \varphi[n] - \frac{2\pi}{N} kn \right\} = \frac{1}{N} \left\{ \sum_{n=0}^{N-1} \varphi[n] - \frac{2\pi}{N} k \sum_{n=0}^{N-1} n \right\} =$$

$$= \frac{1}{N} \left\{ \sum_{n=0}^{N-1} \varphi[n] - \frac{2\pi}{N} k \frac{N(N-1)}{2} \right\} = \frac{1}{N} \left\{ \sum_{n=0}^{N-1} \varphi[n] - \pi k (N-1) \right\}$$

408

(A.16)

409

It follows that: the mean value $\langle \Phi[k] \rangle$ of the k -th DFT value phase can be expressed as a linear

410

combination of all the mean values $\langle \varphi[n] \rangle$ for the sequence phases and the mean value $\langle k \rangle$ of the index

411

$k=0, 1, \dots, N-1$,

412

$$\langle \Phi[k] \rangle \cong \frac{1}{N} \left\{ \sum_{n=0}^{N-1} \langle \varphi[n] \rangle - \pi \langle k \rangle (N-1) \right\}; \quad (\text{A.17})$$

413

then, if the variables $\varphi[n]$ and k are uncorrelated, the variance σ_Φ^2 is a combination of both the

414

variances σ_φ^2 and σ_k^2 ,

415

$$\sigma_\Phi^2 \cong \frac{1}{N^2} \left\{ \sum_{n=0}^{N-1} \sigma_{\varphi[n]}^2 + \pi^2 \sigma_k^2 (N-1)^2 \right\} = \frac{1}{N^2} [N \sigma_\varphi^2 + \pi^2 \sigma_k^2 (N-1)^2]; \quad (\text{A.18})$$

416

finally, as $\sigma_\Phi^2 = \langle \Phi^2[k] \rangle - \langle \Phi[k] \rangle^2$, the mean square value:

417

$$\langle \Phi^2[k] \rangle = \sigma_\Phi^2 + \langle \Phi[k] \rangle^2. \quad (\text{A.19})$$

418

419

Secondly, consider a stochastic complex sequence $x[n]$ consisting of N values [see eq. (A.12)], whose

420

imaginary and real parts are uniform random variables between $-1/(\sqrt{2}N)$ and $+1/(\sqrt{2}N)$, defined by a

421

density of probability

422

$$p_x(x) = \frac{N}{\sqrt{2}} \text{rect}_{1/\sqrt{2}N}(x) = \begin{cases} \frac{N}{\sqrt{2}} & , \quad -\frac{1}{\sqrt{2}N} < x < \frac{1}{\sqrt{2}N} \\ 0 & , \quad \text{elsewhere} \end{cases}, \quad (\text{A.20})$$

423

satisfying the normalization condition of probability:

$$424 \quad \int_{-\infty}^{\infty} p_x(x) dx = \int_{-1/\sqrt{2N}}^{1/\sqrt{2N}} \frac{N}{\sqrt{2}} dx = \frac{N}{\sqrt{2}} \int_{-1/\sqrt{2N}}^{1/\sqrt{2N}} dx = \frac{N}{\sqrt{2}} 2 \int_0^{1/\sqrt{2N}} dx = \frac{N}{\sqrt{2}} 2 \frac{1}{\sqrt{2N}} = 1. \quad (\text{A.21})$$

425 Assume that the imaginary and real parts, $x_I[n]$ and $x_R[n]$, of the complex sequence $x[n]$ (A.12) are
426 two statistical independent variables, so that their joint probability density

$$427 \quad p_{x_I, x_R}(x_I, x_R) = p_{x_I}(x_I) \cdot p_{x_R}(x_R) \Rightarrow \int_{-\infty}^{\infty} \int_{-\infty}^{\infty} p_{x_I, x_R}(x_I, x_R) dx_I dx_R = 1 \quad (\text{A.22})$$

428 can be reduced to the product of the marginal densities:

$$429 \quad p_{x_I}(x_I) = \int_{-\infty}^{\infty} p_{x_I, x_R}(x_I, x_R) dx_R \Rightarrow \int_{-\infty}^{\infty} p_{x_I}(x_I) dx_I = 1. \quad (\text{A.23})$$

$$430 \quad p_{x_R}(x_R) = \int_{-\infty}^{\infty} p_{x_I, x_R}(x_I, x_R) dx_I \Rightarrow \int_{-\infty}^{\infty} p_{x_R}(x_R) dx_R = 1, \quad (\text{A.24})$$

431 Applying the probability theory [Papoulis, 1991]:

432 1. If the joint density of probability for the sequence imaginary and real parts, $x_I[n]$ and $x_R[n]$, is

433 $p_{x_I, x_R}(x_I, x_R)$ (A.22), then the probability density of their ratio (linked to the sequence phase)

434 $y[n] = x_I[n]/x_R[n] (= \text{tg}\varphi[n])$ can be calculated as

$$435 \quad p_y(y) = \int_{-\infty}^{\infty} |x_R| p_{x_I, x_R}(yx_R, x_R) dx_R \stackrel{\text{eq. (A.22)}}{=} \int_{-\infty}^{\infty} |x_R| p_{x_I}(yx_R) p_{x_R}(x_R) dx_R =$$

$$\stackrel{\text{eq. (A.20)}}{=} \int_{-\infty}^{\infty} |x_R| \frac{N}{\sqrt{2}} \text{rect}_{1/\sqrt{2N}}(yx_R) \frac{N}{\sqrt{2}} \text{rect}_{1/\sqrt{2N}}(x_R) dx_R = \frac{N^2}{2} \int_{-1/(\sqrt{2Ny})}^{1/(\sqrt{2Ny})} |x_R| \text{rect}_{1/\sqrt{2N}}(x_R) dx_R = ,$$

$$= \begin{cases} \frac{N^2}{2} \int_{-1/(\sqrt{2N})}^{1/(\sqrt{2N})} |x_R| dx_R = N^2 \int_0^{1/(\sqrt{2N})} x_R dx_R = \frac{1}{4} & , |y| < 1 \\ \frac{N^2}{2} \int_{-1/(\sqrt{2Ny})}^{1/(\sqrt{2Ny})} |x_R| dx_R = N^2 \int_0^{1/(\sqrt{2Ny})} x_R dx_R = \frac{1}{4y^2} & , |y| > 1 \end{cases} \quad (\text{A.25})$$

436

437

satisfying the probability normalization condition:

$$438 \quad \int_{-\infty}^{\infty} p_y(y) dy = \int_{-1}^1 \frac{1}{4} dy + \int_{-\infty}^{-1} \frac{1}{4y^2} dy + \int_1^{\infty} \frac{1}{4y^2} dy = 1. \quad (\text{A.26})$$

439

440

441

2. Introduce the strictly monotonic increasing function $\varphi = f(y) = \text{arctg}(y)$, with continuous first derivative $f'(y) = 1/(1+y^2)$. If the density of probability for the ratio y is $p_y(y)$ (A.25), then the probability density of the sequence phase $\varphi[n] = \text{arctg}(y[n])$ can be calculated as:

$$442 \quad p_\varphi(\varphi) = \frac{p_y(y)}{f'(y)} \Big|_{y=f^{-1}(\varphi)} = p_y(y)(1+y^2) \Big|_{y=\text{tg}\varphi} = p_y(\text{tg}\varphi)(1+\text{tg}^2\varphi) =$$

$$\stackrel{\text{eq. (A.25)}}{=} \begin{cases} \frac{1}{4}(1+\text{tg}^2\varphi) & , |\text{tg}\varphi| < 1 \Leftrightarrow 0 < \varphi < \frac{\pi}{4} \text{ and } \pi - \frac{\pi}{4} < \varphi < \pi \\ \frac{1}{4\text{tg}^2\varphi}(1+\text{tg}^2\varphi) = \frac{1}{4}\left(1 + \frac{1}{\text{tg}^2\varphi}\right) & , |\text{tg}\varphi| > 1 \Leftrightarrow \frac{\pi}{4} < \varphi < \pi - \frac{\pi}{4} \end{cases} \quad (\text{A.27})$$

443

444

satisfying the normalization condition:

$$445 \quad \int_0^\pi p_\varphi(\varphi) d\varphi = \int_0^{\pi/4} \frac{1}{4}(1+\text{tg}^2\varphi) d\varphi + \int_{\pi-(\pi/4)}^\pi \frac{1}{4}(1+\text{tg}^2\varphi) d\varphi + \int_{\pi/4}^{\pi-(\pi/4)} \frac{1}{4}\left(1 + \frac{1}{\text{tg}^2\varphi}\right) d\varphi = 1. \quad (\text{A.28})$$

446

447

It follows that the statistical distribution for the phase $\varphi[n]$ of the stochastic complex sequence $x[n]$ results characterized by the mean value

448

$$\begin{aligned}
\langle \varphi[n] \rangle &= \int_0^{\pi} \varphi p_{\varphi}(\varphi) d\varphi = \\
&= \int_0^{\pi/4} \frac{\varphi}{4} (1 + tg^2 \varphi) d\varphi + \int_{\pi-(\pi/4)}^{\pi} \frac{\varphi}{4} (1 + tg^2 \varphi) d\varphi + \int_{\pi/4}^{\pi-(\pi/4)} \frac{\varphi}{4} \left(1 + \frac{1}{tg^2 \varphi}\right) d\varphi = , \quad (\text{A.29}) \\
&= \frac{1}{16} (\pi - 2 \ln 2) + \frac{1}{16} (3\pi + 2 \ln 2) + \frac{\pi}{4} = \frac{\pi}{2}
\end{aligned}$$

449 then by the mean square value

450

$$\begin{aligned}
\langle \varphi^2[n] \rangle &= \int_0^{\pi} \varphi^2 p_{\varphi}(\varphi) d\varphi = \\
&= \int_0^{\pi/4} \frac{\varphi^2}{4} (1 + tg^2 \varphi) d\varphi + \int_{\pi-(\pi/4)}^{\pi} \frac{\varphi^2}{4} (1 + tg^2 \varphi) d\varphi + \int_{\pi/4}^{\pi-(\pi/4)} \frac{\varphi^2}{4} \left(1 + \frac{1}{tg^2 \varphi}\right) d\varphi = , \quad (\text{A.30}) \\
&= -C + \frac{\pi}{16} (5\pi + \ln 256) \cong \pi
\end{aligned}$$

451 being C the Catalan's constant:

452

$$C = \sum_{m=0}^{\infty} \frac{(-1)^m}{(2m+1)^2} \cong 1. \quad (\text{A.31})$$

453 Finally, by the variance:

454

$$\sigma_{\varphi}^2 = \langle \varphi^2[n] \rangle - \langle \varphi[n] \rangle^2 \cong \pi - \frac{\pi^2}{4}. \quad (\text{A.32})$$

455 Thirdly, consider an index k which assumes N values [see eq. (A.10)],

456

$$k = 0, 1, \dots, N-1, \quad (\text{A.33})$$

457 with uniform probability:

458

$$p_k = \frac{1}{N}. \quad (\text{A.34})$$

460 Similarly to what has been demonstrated by Gauss, the N integer numbers (A.33) satisfy the property

461 for which their sum can be expressed as

462

$$\sum_{k=0}^{N-1} k = \frac{N(N-1)}{2}, \quad (\text{A.35})$$

463 and the sum of their squares in the explicit formula:

464

$$\sum_{k=0}^{N-1} k^2 = \frac{N(N-1)(2N-1)}{6}. \quad (\text{A.36})$$

465 It follows that the statistical distribution of the N integer numbers (A.33)-(A.34) is characterized by

466 the mean value

467

$$\langle k \rangle = \sum_{k=0}^{N-1} k p_k = \frac{1}{N} \sum_{k=0}^{N-1} k \stackrel{\text{eq. (A.25)}}{=} \frac{1}{N} \frac{N(N-1)}{2} = \frac{N-1}{2}, \quad (\text{A.37})$$

468 then by the mean square value

469

$$\langle k^2 \rangle = \sum_{k=0}^{N-1} k^2 p_k = \frac{1}{N} \sum_{k=0}^{N-1} k^2 \stackrel{\text{eq. (A.36)}}{=} \frac{1}{N} \frac{N(N-1)(2N-1)}{6} = \frac{(N-1)(2N-1)}{6}, \quad (\text{A.38})$$

470 and finally by the variance:

471

$$\sigma_k^2 = \langle k^2 \rangle - \langle k \rangle^2 \stackrel{\text{eqs. (A.37)-(A.38)}}{=} \frac{(N-1)(2N-1)}{6} - \left(\frac{N-1}{2}\right)^2 = \frac{N^2 - 1}{12}. \quad (\text{A.39})$$

472 Concluding, for large values of N ,

473

$$\begin{aligned}
\langle \Phi[k] \rangle &\stackrel{eq.(A.17)}{\cong} \frac{1}{N} \left\{ \sum_{n=0}^{N-1} \langle \varphi[n] \rangle - \pi \langle k \rangle (N-1) \right\} = \\
&\stackrel{eq.(A.29)}{=} \frac{1}{N} \left\{ \sum_{n=0}^{N-1} \frac{\pi}{2} - \pi \langle k \rangle (N-1) \right\} = \frac{1}{N} \left[N \frac{\pi}{2} - \pi \langle k \rangle (N-1) \right] = \\
&\stackrel{eq.(A.37)}{=} \frac{1}{N} \left[N \frac{\pi}{2} - \pi \frac{N-1}{2} (N-1) \right] = \frac{\pi}{2} \left[1 - \frac{(N-1)^2}{N} \right] \approx \\
&\stackrel{N \gg 1}{\approx} \frac{\pi}{2} (1-N) \approx -\frac{\pi}{2} N
\end{aligned} \tag{A.40}$$

$$\begin{aligned}
\sigma_{\Phi}^2 &\stackrel{eq.(A.18)}{\cong} \frac{1}{N^2} [N \sigma_{\varphi}^2 + \pi^2 \sigma_k^2 (N-1)^2] \cong \\
&\stackrel{eq.(A.32)}{\cong} \frac{1}{N^2} \left[N \left(\pi - \frac{\pi^2}{4} \right) + \pi^2 \sigma_k^2 (N-1)^2 \right] = \\
&\stackrel{eq.(A.39)}{=} \frac{1}{N^2} \left[N \left(\pi - \frac{\pi^2}{4} \right) + \pi^2 \frac{N^2-1}{12} (N-1)^2 \right] \approx \\
&\stackrel{N \gg 1}{\approx} \frac{\pi^2 (N^2-1)(N-1)^2}{12 N^2} \approx \frac{\pi^2}{12} N^2
\end{aligned} \tag{A.41}$$

$$\langle \Phi^2[k] \rangle \stackrel{eq.(A.19)}{=} \sigma_{\Phi}^2 + \langle \Phi[k] \rangle^2 \stackrel{eqs.(A.40)-(A.41)}{\approx} \frac{\pi^2}{12} N^2 + \frac{\pi^2}{4} N^2 = \frac{\pi^2}{3} N^2, \tag{A.42}$$

479 this appendix has demonstrated a simple formula expressing the phase noise-to-signal ratio due a round-off
480 of FFT processor (the first time on INGV scientific publications, to the best of author knowledge)[see eq.
481 (3.2):
482

$$\frac{\langle |F[k]|^2 \rangle}{\langle |\Phi[k]|^2 \rangle} \stackrel{eq.(A.1)-(A.3),(A.42)}{\approx} \frac{N \frac{1}{3} \cdot 2^{-2n_{FFT}}}{\frac{\pi^2}{3} N^2} = \frac{1}{\pi^2 N 2^{2n_{FFT}}}. \tag{A.43}$$

Acknowledgments.

Dr. A. Settimi would like to thank Drs. C. Bianchi, A. Zirizzotti for the interesting discussions on RESPER probe and Dr. J. A. Baskaradas for the useful hints on literature acculturating about FFT algorithms.

References.

- Arpaia, P., Daponte, P. and Michaeli, L., (1999). Influence of the architecture on ADC error modelling. *IEEE T. Instrum. Meas.*, 48, 956-966.
- Arpaia, P., Daponte, P. and Rapuano, S., (2003). A state of the art on ADC modelling. *Comput. Stand. Int.*, 26, 31-42.
- Björzell, N. and Händel, P., (2008). Achievable ADC performance by post-correction utilizing dynamic modeling of the integral nonlinearity. *Eurasip J. Adv. Sig. Pr.*, 2008, ID 497187 (10 pp).
- Declerk, P., (1995). Bibliographic study of georadar principles, applications, advantages, and inconvenience. *NDT & E Int.*, 28, 390-442 (in French, English abstract).
- Del Vento, D. and Vannaroni, G., (2005). Evaluation of a mutual impedance probe to search for water ice in the Martian shallow subsoil. *Rev. Sci. Instrum.*, 76, 084504 (1-8).
- Dishan, H., (1995). Phase Error in Fast Fourier Transform Analysis. *Mech. Syst. Signal Pr.*, 9, 113-118.
- Grard, R., (1990). A quadrupolar array for measuring the complex permittivity of the ground: application to earth prospection and planetary exploration. *Meas. Sci. Technol.*, 1, 295-301.
- Grard, R., (1990). A quadrupole system for measuring in situ the complex permittivity of materials: application to penetrators and landers for planetary exploration. *Meas. Sci. Technol.*, 1, 801-806.
- Grard, R. and Tabbagh, A., (1991). A mobile four electrode array and its application to the electrical survey of planetary grounds at shallow depth. *J. Geophys. Res.*, 96, 4117-4123.
- Jankovic, D. and Öhman, J., (2001). Extraction of in-phase and quadrature components by IF-sampling. Department of Signals and Systems, Cahlmers University of Technology, Goteborg (carried out at Ericson Microwave System AB).
- Kuffel, J., Malewsky, R. and Van Heeswijk, R. G., (1991). Modelling of the dynamic performance of transient recorders used for high voltage impulse tests. *IEEE T. Power Deliver.*, 6, 507-515.
- Ming, X. and Kang, D., (1996). Corrections for frequency, amplitude and phase in Fast Fourier transform of harmonic signal. *Mech. Syst. Signal Pr.*, 10, 211-221.
- Mojid, M. A., Wyseure, G. C. L. and Rose, D. A., (2003). Electrical conductivity problems associated with time-domain reflectometry (TDR) measurement in geotechnical engineering. *Geotech. Geo. Eng.*, 21, 243-258.
- Mojid, M. A. and Cho, H., (2004). Evaluation of the time-domain reflectometry (TDR)-measured composite dielectric constant of root-mixed soils for estimating soil-water content and root density. *J. Hydrol.*, 295, 263-275.
- Oppenheim, A. V., Schafer, R.W. and Buck, J. R., (1999). *Discrete-Time Signal Processing* (Prentice Hall International, Inc., New York - II Ed.).
- Papoulis, A., (1991). *Probability, Random Variables, and Stochastic Processes* (McGraw-Hill International Editors, Singapore - III Ed.).
- Polge, R. J., Bhagavan, B. K. and Callas, L., (1975). Evaluating analog-to-digital converters. *Simulation*, 24, 81-86.
- Razavi, B., (1995). *Principles of Data Conversion System Design* (IEEE Press, New York).

- Samouëlian, A., Cousin, I., Tabbagh, A., Bruand, A. and Richard, G., (2005). Electrical resistivity survey in soil science: a review. *Soil Till. Res.*, 83, 172-193.
- Sbartai, Z. M., Laurens, S., Balayssac, J. P., Arliguie, G. and Ballivy, G., (2006). Ability of the direct wave of radar ground-coupled antenna for NDT of concrete structures. *NDT & E Int.*, 39, 400-407.
- Settimi, A., Zirizzotti A., Baskaradas, J. A. and Bianchi, C., (2010). Inaccuracy assessment for simultaneous measurement of resistivity and permittivity applying sensitivity and transfer function approaches. *Ann. Geophys-Italy*, 53, 2, 1-19; *ibid.*, Earth-prints, <http://hdl.handle.net/2122/5180> (2009); *ibid.*, arXiv:0908.0641 [physics.geophysics] (2009).
- Settimi, A., Zirizzotti A., Baskaradas, J. A. and Bianchi, C., (2010). Optimal requirements of a data acquisition system for a quadrupolar probe employed in electrical spectroscopy, accepted for publication on *Ann. Geophys-Italy* (23/07/2010); *ibid.*, Earth-prints, <http://hdl.handle.net/2122/5176> (2009); *ibid.*, arXiv:0908.0648 [physics.geophysics] (2009).
- Settimi, A., Zirizzotti A., Baskaradas, J. A. and Bianchi, C., (2010). Design of an induction probe for simultaneous measurements of permittivity and resistivity. *Quaderni di Geofisica*, 79, 26 pp; *ibid.*, Earth-prints, <http://hdl.handle.net/2122/5173> (2009); *ibid.*, arXiv:0908.0651 [physics.geophysics] (2009).
- Tabbagh., A., Hesse, A. and Grard, R., (1993). Determination of electrical properties of the ground at shallow depth with an electrostatic quadrupole: field trials on archaeological sites. *Geophys. Prospect.*, 41, 579-597.
- Vannaroni, G., Pettinelli, E., Ottonello, C., Cereti, A., Della Monica, G., Del Vento, D., Di Lellis, A. M., Di Maio, R., Filippini, R., Galli, A., Menghini, A., Orosei, R., Orsini, S., Pagnan, S., Paolucci, F., Pisani, A. R., Schettini, G., Storini, M. and Tacconi, G., (2004). MUSES: multi-sensor soil electromagnetic sounding. *Planet. Space Sci.*, 52, 67-78.
- Zhang, J. Q. and Ovaska, S. J., (1998). ADC characterization by an eigenvalues method. *Instrumentation and Measurement Technology Conference (IEEE)*, 2, 1198-1202.